Using SCF Metadynamics to Extend Density Matrix Embedding Theory to Excited States

Henry K. Tran,[1] Troy Van Voorhis,[1] and Alex J. W. Thom[2, a)]
[1)] *Department of Chemistry, Massachusetts Institute of Technology, Cambridge, MA 02139, USA*
[2)] *Department of Chemistry, University of Cambridge, Cambridge, UK*

(Dated: 2 June 2019)

A new framework based on density matrix embedding theory (DMET) capable of directly targeting excited electronic states is proposed and implemented. DMET has previously been shown to be an effective method of calculating the ground state energies of systems exhibiting strong static correlation, but has never been applied to calculate excited state energies. In this work, the Schmidt decomposition is applied directly on excited states, approximated by higher lying SCF solutions. The DMET prescription is applied following this Schmidt decomposition allowing for a direct embedding of excited states. Initial results are obtained for a system of multiple hydrogen dimers and the lithium hydride dissociation. We analyze the nature of each part of the excited state DMET calculation and identify challenges. These challenges to the implementation of excited state DMET are discussed and potential suggestions moving forward are recommended.

I. INTRODUCTION

The defining goal of modern electronic structure theory is the ability to describe molecules and materials relevant to the problems of today, with sufficient accuracy and within a feasible amount of computer time. Density functional theory[1,2] (DFT) has become the *de-facto* method for electronic structure calculations on large, extended systems because of the accuracy these calculations can achieve and the low, cubic scaling of these methods. The linear response extension of DFT, time-dependent DFT (TDDFT), is a widely used method to calculate the excited state properties of chemical and material systems.[3–6] DFT and TDDFT are not without flaws. It is well known that DFT is a poor choice to describe the electronic structure of strongly correlated systems[7] and TDDFT, which builds upon that mean-field ground state as a reference, fails to describe many key properties of the system. These include charge transfers, higher potential energy surfaces, vertical excitations, and singlet-triplet transitions.[8]

High level wavefunction methods capable of describing strong correlation for excited states[9,10] scale too highly to effectively describe large systems of interest. It is difficult to study excited states using cheaper Hartree-Fock (HF) theory,[11] but higher lying self-consistent field (SCF) solutions[12] to the HF equations have been compared to excited states. These include Delta SCF (Δ-SCF),[13,14] σ-SCF,[15,16] and SCF metadynamics.[17]

An attractive compromise between the cheap HF and accurate high level methods is the method of embedding, where an impurity, treated at a high level of theory, is embedded within a bath, treated at a low level of theory. Density matrix embedding theory (DMET) has been recently introduced as a successful, self-consistent wavefunction-in-wavefunction embedding method that accurately describes strong correlation.[18,19] DMET utilizes the Schmidt decomposition to reduce the whole space of orbitals to only entangled orbitals from the impurity and bath.[20]

Different approaches have been taken to improving DMET. One direction is to improve the bath calculation. The original papers used HF theory for the bath.[18,19] Hatree-Fock-Bogoliubov Theory,[21] antisymmetrised geminal power (AGP) functions,[22] and block product DMET[23,24] are among the different methods applied to the bath calculation to improve upon the original DMET procedure. Different methods have also been applied to the high level impurity calculation. These include exact methods such as full configuration-interaction (FCI),[18,19] as well as nearly exact methods such as coupled-cluster (CC)[25] and density matrix renormalization group (DMRG).[21,26] Beyond improving the bath and impurity solver, the choice of impurity is also an active area of research. Recent work has shown that an overlapping, instead of disjoint, set of impurities can improve the DMET algorithm.[27–29]

DMET has been successful for the Hubbard model,[18,30] Hubbard-Anderson model,[22] and Hubbard-Holstein model[31] in one dimension. Two dimensional calculations have also been done using DMET for the Hubbard model on the square[18,21,32] and honeycomb[26] lattice and the spin-$\frac{1}{2}$ $J_1 - J_2$ model.[23] As for chemical systems, DMET has found use to study hydrogen rings and sheets,[19,33] carbon polymers, two dimensional boron–nitride sheets, and crystalline diamond.[25] DMET has also been used to define the boundaries in QM/MM simulations[34] and construct basis set contractions.[35] In practice, DMET is not particular to the ground state. It should be possible, in principle, to apply the DMET prescription to excited states, but this large body of work almost exclusively focuses on the ground state. Some initial work has been done to obtain spectral functions through applying the DMET method to a response wave function.[26,36] However, there is currently no literature on directly calculating and embedding multiple electronic states using DMET.

Given the aforementioned success of DMET, it seems there is a lot of unexplored potential in directly embedding excited electronic states. Previously developed methods of targeting higher lying SCF solutions have shown to be effective ap-

[a)] Electronic mail: ajwt3@cam.ac.uk

proximations of excited states[14,37] or good starting points to excited state calculations.[38] DMET is a method which builds upon and improves mean-field approximations to ground state wavefunctions and we expect that its success will translate to excited states by using higher lying SCF solutions.

In this work, we discuss a generalization of the DMET method to embed excited states. We approach this by using higher lying SCF states as approximations to excited electronic states. This provides a better starting point for the impurity calculation to capture characteristics of the excited state. Since FCI is used for the impurity calculation, it naturally returns excited states local to the impurity. Piecing together each excited impurity calculation will provide a better description of the full system excited state.

This paper is organized as follows. Section II reviews the prerequisite theory of DMET. The Schmidt decomposition is discussed formally and in context of a mean-field eigenstate. The DMET prescription is briefly reviewed. Section III introduces our modification of the DMET prescription, generalized to be applicable to excited eigenstates. Section IV discusses the systems of interest and the computational details. We demonstrate the effectiveness of excited state DMET in matching exact calculations, even in seemingly difficult extremes of the potential energy surface, and discuss the nuances and limitations of the method. In Section V, we conclude this work by summarizing the key successes and pitfalls of excited state DMET and future directions to improve the method.

II. BACKGROUND

In this section, we review the prerequisites to DMET and the DMET algorithm as presented in the original papers.[18,19]

A. Schmidt-Decomposition

The equations of DMET rely on the ability to partition a larger system into a smaller subsystem, referred to as the impurity, and the rest of the system, referred to as the bath. Consider a system described by a Hilbert space H of dimension d. Suppose the Hilbert space is divided into two smaller Hilbert spaces, H_A and H_B, with dimensions d_A and d_B respectively such that H can be represented as the direct product of H_A and H_B.

$$H = H_A \otimes H_B \tag{1}$$

Let $\{|a_i\rangle\}$ and $\{|b_j\rangle\}$ be the bases of H_A and H_B respectively. Any wave function, $|\Psi\rangle$, in H can be expressed in the direct product basis as[39]

$$|\Psi\rangle = \sum_{i=1}^{d_A}\sum_{j=1}^{d_B} C_{ij}\,|a_i\rangle \otimes |b_j\rangle \tag{2}$$

where C_{ij} are obtained as

$$C_{ij} = \left(\langle a_i| \otimes \langle b_j|\right)|\Psi\rangle \tag{3}$$

Defining the coefficient matrix as the $d_A \times d_B$ matrix $\mathbf{C}$ with elements C_{ij}, the singular value decomposition (SVD) of $\mathbf{C}$ can be written as

$$\mathbf{C} = \mathbf{U}\Lambda\mathbf{V}^\dagger \tag{4}$$

where $\mathbf{U}$ is a $d_A \times d_A$ orthogonal matrix and $\mathbf{V}$ is a $d_B \times d_B$ orthogonal matrix. Λ is a $d_A \times d_B$ diagonal matrix with the singular values of $\mathbf{C}$ along the diagonal. The elements of $\mathbf{C}$ are given by

$$C_{ij} = \sum_{k=1}^{d_m} U_{ik}\Lambda_{kk}V^*_{jk} \tag{5}$$

where $d_m = \min(d_A, d_B)$. Inserting this expression into Equation (2) yields

$$|\Psi\rangle = \sum_{i=1}^{d_A}\sum_{j=1}^{d_B}\sum_{k=1}^{d_m} U_{ik}\Lambda_{kk}V^*_{jk}\,|a_i\rangle \otimes |b_j\rangle \tag{6}$$

$$|\Psi\rangle = \sum_{k=1}^{d_m}\Lambda_{kk}\left(\sum_{i=1}^{d_A} U_{ik}\,|a_i\rangle\right) \otimes \left(\sum_{j=1}^{d_B} V^*_{jk}\,|b_j\rangle\right) \tag{7}$$

$$|\Psi\rangle = \sum_{k=1}^{d_m}\Lambda_{kk}\,|\alpha_k\rangle \otimes |\beta_k\rangle \tag{8}$$

where

$$|\alpha_k\rangle = \sum_{i=1}^{d_A} U_{ik}\,|a_i\rangle \tag{9}$$

$$|\beta_k\rangle = \sum_{j=1}^{d_B} V^*_{jk}\,|b_j\rangle \tag{10}$$

Equation (8) is known as the Schmidt decomposition.[39] Note that the states $|\alpha_k\rangle$ span only H_A and $|\beta_k\rangle$ span only H_B. This expansion is exact, but contains only d_m terms as opposed to $d_A \cdot d_B$ terms of Equation (2). The singular values Λ_{kk} represent the entanglement between states $|\alpha_k\rangle$ and $|\beta_k\rangle$ and take on values between 0 and 1.[40]

B. Schmidt-Decomposition of HF Wavefunctions

Although Equation (8) is exact, it is usually not possible to know $|\Psi\rangle$ beforehand. In practice, one can approximate $|\Psi\rangle$ as the Slater determinant that solves the HF equations.[41]

$$\Psi'(\mathbf{s}) = \frac{1}{\sqrt{n!}}\det\begin{pmatrix}\phi_1(\mathbf{x}_1) & \cdots & \phi_n(\mathbf{x}_1)\\ \vdots & \ddots & \vdots\\ \phi_1(\mathbf{x}_n) & \cdots & \phi_n(\mathbf{x}_n)\end{pmatrix} \equiv |\phi_1 \cdots \phi_n| \tag{11}$$

In Equation (11), ϕ_i are generally taken to be atomic spin-orbitals and $\mathbf{x}_i$ is a variable denoting spatial and spin coordinates.

After obtaining a self-consistently optimized Slater determinant from solving the HF equations, one can obtain the one-particle reduced density matrix (1-RDM), $\mathbf{P}$, with elements

$$\mathbf{P}_{ij} = \langle \hat{a}_i^\dagger \hat{a}_j \rangle \tag{12}$$

where $\hat{a}_i^\dagger$ and $\hat{a}_i$ are the creation and annihilation operators for ϕ_i. We can define an impurity (A) and bath (B) HF density by taking only the sub-matrix containing orbitals in the impurity or bath.

$$\mathbf{P}^A = \mathbf{P}[\{i \in A\}, \{i \in A\}] \tag{13}$$

$$\mathbf{P}^B = \mathbf{P}[\{i \in B\}, \{i \in B\}] \tag{14}$$

The impurity (bath) density can be diagonalized into a diagonal matrix, Λ^A (Λ^B). Let $\mathbf{U}^A$ ($\mathbf{U}^B$) denote the matrix of eigenvectors for $\mathbf{P}^A$ ($\mathbf{P}^B$).

$$\Lambda^A = (\mathbf{U}^A)^{-1} \mathbf{P}^A \mathbf{U}^A \tag{15}$$

$$\Lambda^B = (\mathbf{U}^B)^{-1} \mathbf{P}^B \mathbf{U}^B \tag{16}$$

The case of a mean-field HF determinant, the many electron states presented in Equations (9) and (10) span the same space as the one electronic states used to form the HF determinant. We can formulate our Schmidt decomposed impurity and bath states as

$$|\alpha_k\rangle = \sum_{i=1}^{d_A} \mathbf{U}_{ik}^A \left|\phi_i^A\right\rangle \tag{17}$$

$$|\beta_k\rangle = \sum_{j=1}^{d_B} \mathbf{U}_{jk}^B \left|\phi_j^B\right\rangle \tag{18}$$

ϕ_i^A (ϕ_j^B) denote the atomic orbitals in the impurity (bath). Hence, defining the impurity and bath Schmidt space equates to a rotation of atomic orbitals.

Assuming $d_A < d_B$, further classification of the bath states can be made. The eigenvalues of $\mathbf{P}^B$ can be divided into

1. Between 0 and 1. These are active bath orbitals.
2. Equal to 1. These are core orbitals.
3. Equal to 0. These are virtual orbitals.

There are d_A active bath orbitals and these will be denoted $|\beta_i\rangle$. There are $n_{\text{occ}} - d_A$ core orbitals, where n_{occ} refers to the number of occupied orbitals. These will be referred to as core states and denoted $\left|\gamma_p\right\rangle$. They serve the same role as core orbitals in complete active space (CAS) calculations. There are $m - n_{\text{occ}} - d_A$ virtual orbitals, where m denotes the total number of orbitals. These will be denoted $|\varepsilon_a\rangle$. These serve the same role as virtual orbitals in CAS calculations. For the rest of the discussion, the indexes $i, j, k, l, \ldots$ will belong to impurity and bath states. The orbitals are assumed to be ordered so that all impurity states come before bath states. The indexes $a, b, \ldots$ will belong to virtual states and the indexes $c, d, \ldots$ will belong to core states. All states in the embedding basis will be indexed by $p, q, r, s, \ldots$. The total HF wave function is thus represented as

$$\left|\Psi^{\text{HF}}\right\rangle = \left(\sum_{i=1}^{d_m} \Lambda_{ii} |\alpha_i\rangle \otimes |\beta_i\rangle\right) \otimes |\gamma_1 \gamma_2 \cdots| \otimes |\varepsilon_1 \varepsilon_2 \cdots| \tag{19}$$

C. Summary of DMET

In this section, we briefly discuss the DMET method. For a more detailed discussion, we refer the readers to the original DMET papers.[18,19]

In DMET, the system is tiled into a set of impurities, denoted A^x, indexed by x. For each A^x, there is the corresponding bath, denoted B^x.

The DMET method begins by solving the full system at a low level of theory. In order to account for entanglement between the bath and impurity in this calculation, a correlation potential, $\hat{u}$, is added to the electronic Hamiltonian.

$$\hat{\mathscr{H}}' = \hat{\mathscr{H}} + \hat{u} \tag{20}$$

$\hat{u}$ represents the local correlation felt by the impurity and has the form

$$\hat{u} = \sum_x \sum_{ij \in A^x} u_{ij}^x \hat{c}_i^\dagger \hat{c}_j \tag{21}$$

where $\hat{c}_i^\dagger$ and $\hat{c}_i$ are the creation and annihilation operators in the Schmidt space basis.

The impurity Hamiltonian, for each impurity x, can be defined as

$$\hat{\mathscr{H}}^x = \hat{P}^x \hat{\mathscr{H}} \hat{P}^x - \mu_{\text{glob}} \sum_{i \in A^x} \hat{c}_i^\dagger \hat{c}_i \tag{22}$$

where

$$\hat{P}^x = \sum_{ij} \left|\alpha_i^x\right\rangle \left|\beta_j^x\right\rangle \left\langle \alpha_i^x \right| \left\langle \beta_j^x \right| \tag{23}$$

is the projection operator that projects the Hamiltonian onto the impurity space and μ_{glob} is a local chemical potential, independent of fragment x that is chosen to minimize the following cost function.

$$\mathrm{L}^\mu(\mu_{\text{glob}}) = \left(\left[\sum_x \sum_{i \in A^x} \mathbf{P}_{ii}^x(\mu_{\text{glob}})\right] - n_{\text{occ}}\right)^2 \tag{24}$$

$\mathbf{P}^x$ is the 1-RDM of the solution to the impurity Hamiltonian in the Schmidt space basis as defined in Equation (12) with $\hat{a}_i$ replaced by the corresponding Schmidt space creation operator $\hat{c}_i$.

The correlation potential, $\hat{u}$, is chosen to match the 1-RDM obtained from the full system calculation with the 1-RDMs of each fragment on each fragment site. All off-diagonal and diagonal elements are matched. This is accomplished by minimizing the following cost function.

$$\mathrm{L}^u(u) = \sum_x \sum_{ij \in A^x} \left(\mathbf{P}_{ij}^x - \mathbf{P}_{ij}^{\text{HF}}(u)\right)^2 \tag{25}$$

Define the two particle reduced density matrix (2-RDM) as

$$\Gamma_{ijkl} = \langle \hat{c}_i^\dagger \hat{c}_j^\dagger \hat{c}_l \hat{c}_k \rangle \tag{26}$$

and the 1-RDM as in Equation (12). For each impurity, with 1-RDM $\mathbf{P}^x$ and 2-RDM Γ^x, the energy of the impurity is

$$E^x = \sum_{i\in A^x}\left[\sum_{j\in A^x\cup B^x}\frac{2\tilde{h}^x_{ij}+\sum_c\left(2\tilde{V}^x_{icjc}-\tilde{V}^x_{iccj}\right)}{2}\mathbf{P}^x_{ij} + \frac{1}{2}\sum_{jkl\in A^x\cup B^x}\tilde{V}_{ijkl}\Gamma^x_{ijkl}\right] \tag{27}$$

where $\tilde{h}^x_{pq}$ and $\tilde{V}^x_{pqrs}$ are the one and two electron integrals in the Schmidt space basis (in physicist notation), respectively. The total DMET energy is given by

$$E = \sum_x E^x + E_{\text{nuc}} \tag{28}$$

where E_{nuc} is the nuclear repulsion energy.

III. EXCITED STATE DMET

In principle, any eigenstate can be chosen for the Schmidt decomposition of Equation (2). Although Section II C assumed a ground eigenstate, the theory can be applied to any eigenstate and this work will attempt to apply the theory to embed excited eigenstates directly. The generalization to excited state DMET is conceptually straightforward. The methodology in Section II C will be applied to higher lying solutions to the impurity Hamiltonian and the full system Hamiltonian. The self-consistency condition can be achieved by matching the 1-RDMs of these higher lying solutions instead of the lowest solution. There are two difficulties that arise in embedding higher lying eigenstates. The first is that the original full system wavefunction must accurately approximate the excited state we are targeting, and this is difficult for mean-field methods. The second is that the ground state impurity solution may no longer be the most appropriate choice of eigenstate to represent the impurity. We explore these difficulties in this section.

A. Multiple State DMET

Each impurity calculation in DMET requires two electronic structure calculations. First, it requires a bath calculation that describes how the impurity is entangled to the bath, affecting the impurity calculation. Second, it requires the impurity calculation itself.

The choice of the bath state is important because it defines the Schmidt space that significantly affects the impurity calculation. The ground state HF solution does an exceptional job of choosing a good Schmidt basis. However, we cannot expect the ground state HF solution to provide an accurate Schmidt basis for excited states. In this paper, we will choose higher lying SCF solutions to the RHF equations using a method inspired by metadynamics.[17] The details of this method are detailed in Section III C.

In many systems of interest, the excited state has an open shell structure. We may expect that solutions obtained from a method such as restricted open shell HF (ROHF),[42] or unrestricted HF (UHF),[43] as the starting point for a DMET calculation will provide a better Schmidt space than restricted closed shell HF. In this study, we restrict ourselves to closed shell RHF for simplicity, but find the closed shell RHF solutions to be sufficient. The method described in this work is easily generalizable to UHF or ROHF solutions and this is certainly a useful pursuit for future work.

The choice of impurity state is also important. The impurity Hamiltonian, in principle, contains in its eigenspectrum the eigenvalue of the wavefunction that was used in the Schmidt decomposition. For the ground state wavefunction, the ground state energy is also the ground state energy of the impurity Hamiltonian. For an excited state wavefunction, it is not clear which impurity eigenvalue is the one we are trying to target. The difficulty is in deciding which locally excited impurity state best resembles the excited state of the full system on the impurity.

With the necessity to allow freedom in which bath and impurity states to select, we summarize DMET in terms of embedding multiple electronic states. For each fragment x, we must choose a bath and impurity state. We denote the choice of bath excitation by n^B and impurity excitation by n^A. We emphasize that n^B and n^A depend on x. The equations in Section II C are modified to depend on both of these choices.

For each choice of bath excitation, n^B, the full system Hamiltonian is solved and the 1-RDM of the n^B eigenstate, $\mathbf{P}^{\text{HF}}_{n^B}(\hat{u})$, is obtained. The Schmidt decomposition is performed for this eigenstate following the procedure described in Section II B.

Within this Schmidt basis, dependent on n^B, the impurity Hamiltonian can be written as

$$\hat{\mathscr{H}}^x_{n^B} = \sum_{ij}\left[\tilde{h}^x_{n^B,ij}+\sum_{c\in\text{core}}\left(2\tilde{V}^x_{n^B,icjc}-\tilde{V}^x_{n^B,iccj}\right)\right]\hat{c}^\dagger_i\hat{c}_j + \frac{1}{2}\sum_{ijkl}\tilde{V}^x_{n^B,ijkl}\hat{c}^\dagger_i\hat{c}^\dagger_j\hat{c}_l\hat{c}_k - \mu_{\text{glob}}\sum_{i\in A^x}\hat{c}^\dagger_i\hat{c}_i \tag{29}$$

where the subscript n^B has been added to the one and two electron integrals, indicating that these integrals are in the Schmidt basis obtained from the Schmidt decomposition of the n^B bath eigenstate.

Note that the choice of impurity eigenstate, n^A, for the impurity is not yet relevant, and will only be relevant for the matching of 1-RDMs. The choice function for the bath serves the purpose of both deciding which density to match and defining the Schmidt space for the impurity calculation.

Multiple solutions to the impurity Hamiltonian can be obtained, as well as their 1-RDM and 2-RDM. We select the n^A eigenstate to represent our impurity, and obtain the 1-RDM and 2-RDM: $\mathbf{P}^x_{n^B;n^A}$ and $\Gamma^x_{n^B;n^A}$. The first label is the bath eigenstate used to define the Schmidt space in which the impurity calculation was done. The second label is the impurity eigenstate from the impurity calculation used to obtain the RDMs.

The impurity energy is

$$E^x = \sum_{i\in A^x}\left[\sum_{j\in A^x\cup B^x}\frac{2\tilde{h}^x_{n^B,ij}+\sum_c\left(2\tilde{V}^x_{n^B,icjc}-\tilde{V}^x_{n^B,iccj}\right)}{2}\mathbf{P}^x_{n^B;n^A,ij}+\frac{1}{2}\sum_{jkl\in A^x\cup B^x}\tilde{V}^x_{n^B,ijkl}\Gamma^x_{n^B;n^A,ijkl}\right] \tag{30}$$

The cost function is modified to use the proper 1-RDM in the matching conditions.

$$\mathrm{L}^{\mu}(\mu_{\mathrm{glob}}) = \left(\left[\sum_x\sum_{i\in A^x}\mathbf{P}^x_{n^B;n^A,ii}(\mu_{\mathrm{glob}})\right]-n_{\mathrm{occ}}\right)^2 \tag{31}$$

$$\mathrm{L}^{u}(u) = \sum_x\sum_{ij\in A^x}\left(\mathbf{P}^x_{n^B;n^A,ij}-\mathbf{P}^{\mathrm{HF}}_{n^B,ij}(u)\right)^2 \tag{32}$$

B. State Selection in DMET

In this work, we suggest the following method of selecting n^B and n^A. The choice of n^B relies on knowledge of how well the mean-field method of choice approximates the excited state and this choice should be easier for mean-field methods designed to target specific excited states. In our case, we are using higher lying SCF solutions to the RHF equations, found exhaustively, so we expect the first excited state to lie somewhere between the lowest and first excited RHF solution. We will pick between either of these solutions and use selected full system state for every fragment.

For the choice of n^A, we compute multiple solutions to the impurity Hamiltonian and obtain multiple 1-RDMs. We choose the solution whose 1-RDM best matches some reference 1-RDM, $\mathbf{P}^{\mathrm{ref}}$, on the impurity.

$$n^A = \min_n\sum_{ij\in A^x}\left[\mathbf{P}^x_{n^B;n,ij}-\mathbf{P}^{\mathrm{ref}}_{ij}\right]^2 \tag{33}$$

$\mathbf{P}^{\mathrm{ref}}$ should be obtained cheaply and it is reasonable to use $\mathbf{P}^{\mathrm{HF}}_{n^B}$. However, in this work, since we are starting from a closed shell RHF solution, we find it better to use Δ-SCF solutions[14] to the UHF equations as the reference.

C. SCF Metadynamics

The impurity calculation, done using exact diagonalization, will naturally yield higher energy solutions. However, RHF is a ground state variational theory and lacks an obvious method to obtain higher lying electronic states.

For this work, the higher lying bath solutions will be found as higher energy solutions to the SCF method, and these will be found using SCF metadynamics.

Metadynamics is a method used in molecular dynamics simulations to bias the convergence of the simulation to a different minimum.[44] When a dynamical simulation has converged, a biasing potential in the form of a Gaussian is added to the total energy, centered at the converged geometry. When the simulation is ran again, the simulation will converge away from the previously found minimum allowing for a more complete search of the potential energy surface.

A modification will be made to the SCF equations that achieves the same effect as metadynamics, when considering SCF convergence. It is important to note that each solution is uniquely described by its 1-RDM. For the rest of this section, ${}^m\mathbf{P}$, ${}^n\mathbf{P}$, ... will denote the 1-RDM of different solutions.

First, the space of 1-RDMs can be considered a vector space equipped with an inner product. For this paper, the inner product will be defined as

$$2\langle {}^m\mathbf{P}, {}^n\mathbf{P}\rangle = \sum_{\mu\nu}{}^m\mathbf{P}_{\mu\nu}{}^n\mathbf{P}_{\nu\mu} \tag{34}$$

The metric between two solutions, $d^2_{mn} = \langle {}^m\mathbf{P}-{}^n\mathbf{P}, {}^m\mathbf{P}-{}^n\mathbf{P}\rangle$, can be written as

$$d^2_{mn} = N - \sum_{\mu\nu}{}^m\mathbf{P}_{\mu\nu}{}^n\mathbf{P}_{\nu\mu} \tag{35}$$

where N is the number of electrons. This definition is equivalent to

$$d^2_{mn} = \sum_i\left\langle {}^m\psi'\right|\left(\left|{}^m\phi_i\right\rangle\left\langle {}^m\phi_i\right| - \left|{}^n\phi_i\right\rangle\left\langle {}^n\phi_i\right|\right)\left|{}^n\psi'\right\rangle \tag{36}$$

where ${}^n\psi'$ refers to the n solution to the electronic problem, in the form of a Slater determinant formed from spin orbitals ${}^n\phi_i$. It is seen that $d^2_{mm} = 0$ as it should. Moreover,

$$\sum_{\mu\nu}{}^m\mathbf{P}_{\mu\nu}{}^n\mathbf{P}_{\nu\mu} = \sum_{ij}\left\langle {}^m\phi_i\middle|{}^n\phi_j\right\rangle\left\langle {}^n\phi_j\middle|{}^m\phi_i\right\rangle \tag{37}$$

is bounded between 0 and n. Hence, d^2_{mn} is also bounded between 0 and n and is positive definite. Moreover, every term in the sum on the right-hand side of Equation (37) is a complex norm and hence, they are all real. It follows that $d^2_{mn} = (d^2_{mn})^*$, fulfilling conjugate symmetry. This definition of the metric can be intuitively understood as a measure of different electrons between two solutions. For example, if m and n differed by exactly k spin orbitals, $d^2_{mn} = k$.

Now that a metric has been defined between two different solutions. A modified Lagrangian can be implemented which biases the energy away from previously found solutions. The new modified Lagrangian expression, obtained by adding a Gaussian biasing potential the HF energy, is defined as

$$\tilde{E} = E + \sum_n N_n e^{-\lambda_n d^2_{0n}} \tag{38}$$

Here, n indexes all previously converged solutions and d^2_{0n} denotes the metric between the current density matrix and n. N_n

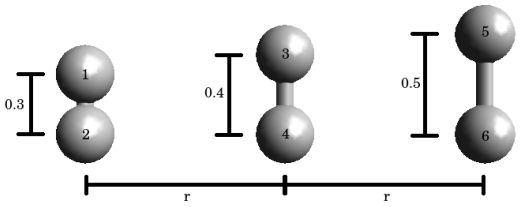

FIG. 1. Geometry of the H_2 dimers system. The bond lengths on each dimer are 0.3, 0.4, and 0.5 Å. The distance between each dimer, labeled r, is varied in the following calculations.

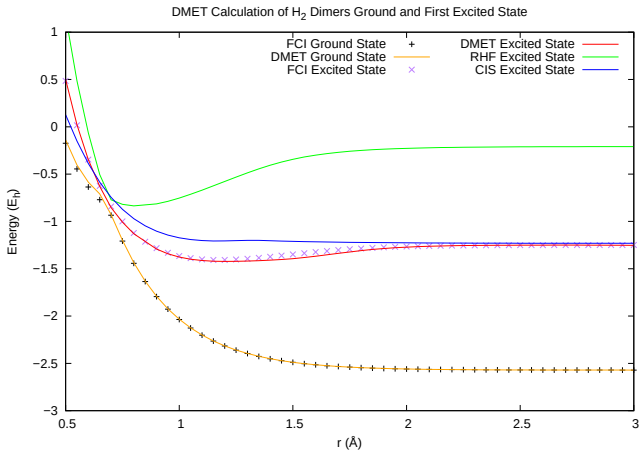

FIG. 2. The FCI ground state energy (black), FCI first singlet excited state energy (purple), DMET ground state energy (orange), and DMET first excited state energy (red) of the model triple dimer system. Singlet excited state energies using RHF (green) and CIS (blue) are also plotted for comparison.

and λ_n control the height and width of the Gaussian respectively, and are varied throughout the calculation to make the Gaussian larger if a new solution is not found. The Fock matrix can be considered a derivative of the energy with respect to the density matrix

$$\mathbf{F}_{\mu\nu} = \frac{\partial E}{\partial \mathbf{P}_{\mu\nu}} \tag{39}$$

Taking the derivative of $\tilde{E}$ gives the modified Fock matrix to be solved, $\tilde{\mathbf{F}}$.

$$\tilde{\mathbf{F}}_{\mu\nu} = \mathbf{F}_{\mu\nu} + \sum_n {}^n\mathbf{P}_{\mu\nu} N_n \lambda_n e^{-\lambda_n d_{0n}^2} \tag{40}$$

The algorithm for metadynamics follows the same steps the typical SCF method, except that the SCF calculation is done twice. The first time, called the biased SCF, uses $\tilde{\mathbf{F}}$ in Equation (40) instead of $\mathbf{F}$. For the second SCF run, called the unbiased SCF, $\mathbf{F}$ is used, but the starting 1-RDM is the solution to the biased SCF run. The bias is removed to allow the SCF method to converge to a true stationary point.

IV. RESULTS

A. Hydrogen Dimers Results

The first system is a system of three H_2 dimers, each with a different bond length. We vary the distance between the dimers, r. The exact geometry of the system of interest is shown in Figure 1. We will refer to the longest dimer as the right dimer, the second longest dimer as the middle dimer, and the shortest dimer as the left dimer, in reference to Figure 1. The hydrogens are numbered 1-6, and this will be the numbering scheme used for the rest of this paper.

This particular system was chosen because it is easy to identify the character of the excited states and it tests DMET in the obvious limit of large r, where all electronic properties are local to each dimer and an embedding method is expected to be perfect, and at small r, where there is significant coherence between each dimer and it will be challenging for DMET to describe.

Electron integrals were computed in a STO-3G basis[45] with Löwdin symmetric orthogonalization[46] using PySCF.[47] FCI energies are computed for comparison, also using PySCF. In the following calculations, r is varied between 0.50 Å and 3.00 Å in steps of 0.05 Å.

All DMET calculations using the method described in Section III were done on in-house software utilizing the Eigen library for matrix algebra.[48] For all calculations, a tiling of the system into three impurities was done. Impurity 1 chooses the left dimer as the impurity. Impurity 2 chooses the middle dimer as the impurity. Impurity 3 chooses the right dimer as the impurity. The DMET calculations are done without optimizing the correlation potential, which we set to be zero: $\hat{u} = 0$. This is because our system is approaching the limit of non-interacting dimers at large r and each dimer is taken as an impurity. In this case, for an FCI-in-HF embedding, the DMET correlation potential actually spoils the calculation. This is because the FCI impurity calculation is already exact, but since a mean-field density matrix cannot match an FCI density matrix, the matching condition spoils the exact calculation. This was discussed in more detail with numerical examples in other literature.[22]

1. *Ground State Calculation*

The FCI energies of the two lowest lying singlet electronic states are plotted in Figure 2. A ground state DMET calculation is done on the dimers systems. The lowest SCF solution is used as the bath solution. The result is plotted in Figure 2.

The agreement between FCI and DMET is exceptionally good, as is usually expected in these systems. It is interesting to note that at $r > 0.65$ Å, the FCI and DMET solution for the ground state shows that the dimers are no longer coupled. From this point onwards, the decrease in energy is purely a result of decreasing coulomb repulsion between the hydrogen

nuclei as they are pulled apart.

2. First Excited State Calculation

We observe immediately that there is a metastable bound state for the first excited state, unlike the ground state. The optimum separation lies at $r = 1.15$ Å as can be seen in Figure 2. As was discussed in Section IV A 1, by choosing n^B as the lowest HF solution, the dimers become uncoupled. Hence, any DMET calculation embedded within the lowest HF solution would show a repulsive decay and cannot reproduce the first excited state.

For the first excited state, we choose the first excited SCF solution for $r > 0.65$ Å and the lowest SCF solution for $r \leq 0.65$ Å, because the SCF solutions cross at that point. The reference density matrix in Equation (33) was chosen to be the first excited Δ-SCF solution to the UHF equations. An excited state DMET calculation was done with this choice of bath state and reference 1-RDM, at a reference geometry before and after the avoided crossing. The solution was followed to produce the curve in those two regions.

We compute the first excited state energy along different values of r and plot the results in Figure 2. We see good agreement between DMET and FCI along most of the curve. The only difference in the DMET calculation is the curvature around $r = 1.5$ Å. Even with this curvature, both calculations predict nearly the same minimum, with the DMET calculation slightly overestimating the minimum. To compare with typical, low scaling excited state methods, we have also plotted the first singlet excited state from SCF metadynamics (the state used for the embedding) and configuration interactions singles (CIS) in that same figure. We find that neither of these calculations reproduce the energy or shape of the curve as well as our excited state DMET implementation. DMET recovers a significant amount of correlation in the first excited state.

B. Hydrogen Dimers Discussion

1. Localized and Delocalized Excitations

We turn our attention to the nature of the excitation in this dimer system, based on the exact FCI calculation. The occupied natural orbitals and their occupation at $r = 0.50$ Å, $r = 1.25$ Å, and $r = 3.00$ Å are pictured in Figure 3.

Figure 3 shows that the excitation is initially spread among all three H_2 dimers. As the separation between the dimers increases, the excitation localizes onto the middle and right dimers. At longer separations, the excitation is localized to only the right dimer.

One would expect that an embedding method, which takes each dimer as its fragments, ought to be perfect at large r. We observe good agreement between DMET and FCI at not only this limit, but even at smaller r values as well. It is surprising that DMET also captures the cases where the excitation is delocalized outside the boundary of its impurities.

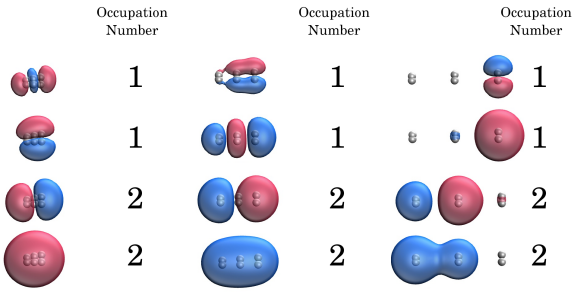

FIG. 3. The occupied natural orbitals and their occupation numbers of the triple H_2 dimer system at $r = 0.50$ Å (left), $r = 1.25$ Å (middle), and $r = 3.00$ Å (right). These orbitals are obtained from the FCI solution for the first singlet excited state at each of these geometries.

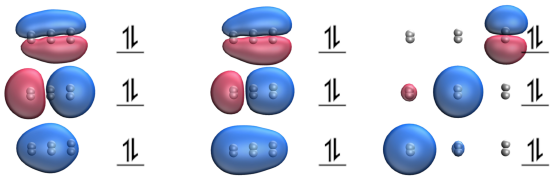

FIG. 4. The occupied molecular orbitals for the SCF solutions chosen for the excited state DMET calculation at $r = 0.50$ Å (left), $r = 1.25$ Å (middle), and $r = 3.00$ Å (right). Specifically, these are the lowest, second lowest, and second lowest SCF solutions at these geometries, respectively.

2. Assessing State Selection

We found in this system that the simple choice of ground RHF solution for the ground DMET calculation and first excited RHF solution for the first excited DMET calculation to be effective. In this section, we explore the nature of these RHF solutions compared to the true excitations in an attempt to create a better metric.

The occupied molecular orbitals (MO) of the SCF solution we chose for the calculation at $r = 0.50$ Å, $r = 1.25$ Å, and $r = 3.00$ Å are shown in Figure 4. We find that the MOs of the SCF calculation shows some similarities with the natural orbitals of the FCI calculation in Figure 3. In this work, we are restricting ourselves to closed shell RHF solutions for the full system calculation. It is unusual for a closed shell solution to accurately represent an open shell state, but our results in this paper show that it is possible in DMET. We will see in Section IV B 3 that the impurity calculations recover open shell character.

We find the first excited RHF solution produces populations that agree with the FCI populations better than any lower lying RHF solution. For reference, we list the populations on each hydrogen atom as obtained from the FCI calculation and the five lowest SCF solutions at $r = 1.00$ Å in Table I. We also calculate the distance metric, as given in Equation (35). We find that the true FCI solution is roughly equidistant from the lowest and second lowest SCF solution. This makes sense, as we would probably expect the true open shell excited state to

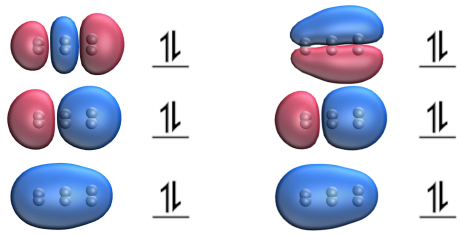

FIG. 5. The occupied molecular orbitals of the lowest (left) and second lowest (right) SCF solutions of the triple dimer system at $r = 1.25$ Å.

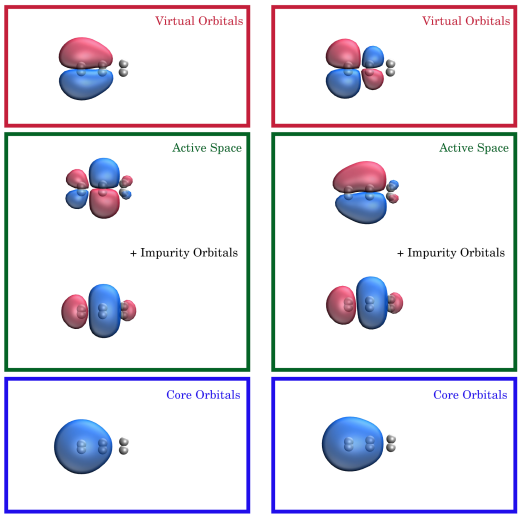

FIG. 6. The bath orbitals obtained from the Schmidt Decomposition of the lowest (left) and second lowest (right) SCF solutions pictured in Figure 5. The orbitals in the impurity are not pictured, but are included in the active space.

be somewhere between the first and second closed shell RHF solutions. To better visualize the effect of choosing between the lowest and second lowest RHF state, the MOs of these eigenstates are plotted in Figure 5 and the Schmidt spaces obtained from each eigenstate are shown in Figure 6. It may be worth approximating the populations from a method more accurate than mean-field, that is still cheap.

In this small hydrogen dimer system, the mapping of ground SCF solution for ground state calculation and first excited SCF solution for first excited state was successful. This success will likely not carry over to larger systems. Continuing with the use of SCF metadynamics will require chemical intuition about which excited state RHF solution is the proper choice, and this is a setback for expanding this method.

To this point, we note that SCF metadynamics for closed shell RHF is stochastic and does a poor job of targeting specific eigenstates, and does not accurately represent open shell states. To explore larger molecules, we should move beyond this. A theory more generalized, such as UHF or ROHF, applied with a method better designed to target specific excited states, such as Δ-SCF or σ-SCF, should make the choice of bath state easier. It will be interesting to see how these alternative, state targeting methods handle this ambiguity.

As for selecting the impurity state, matching impurity 1-RDMs against higher lying UHF solutions found using Δ-SCF as described in Equation (33) was found to be successful. At least in this system, UHF was adequate in providing the reference 1-RDM. The impurity solutions are distinct enough that the reference 1-RDM is allowed a large margin of error, so long as it is qualitatively accurate. However, in other more complex systems, UHF is not even qualitatively accurate. In these cases, this excited state embedding will have problems without finding a better method to produce the reference 1-RDM.

The comparison of 1-RDMs as a metric is quite trivial and is unfortunately closely tied with producing an accurate full system calculation. Moving forward, it would be highly beneficial to have different metric that can be used to distinguish between impurity states. Such a metric could be a substantial landmark for excited state embedding. Still, the use of the trivial metric in this metric serves as a demonstration that excited state embedding can be successful, and that further work in finding a metric that is easier to improve could be put to good use.

3. *Open Shell Character from Closed Shell Bath*

Our implementation of excited state DMET starts from a closed shell RHF solution, but it was able to predict the energy of an open shell state. In this section, we demonstrate that the open shell character of our result arises from the impurity calculation, rather than the full system calculation.

While it seems concerning that our implementation of excited state DMET starts from a closed shell solution, we note that purpose of this solution is to provide the Schmidt space for the impurity calculation. The impurity calculation itself is what dictates the energy of the targeted state. Figure 7 shows the natural orbitals and their occupation numbers of the impurity calculation at $r = 1.25$ Å for the right impurity. Figure 8 shows the same at $r = 3.00$ Å. We note that the character of the impurity state is that of an open shell state, as indicated by the occupation numbers. Hence, although our full system method is incapable of open shell character, our impurity method (FCI) is capable of such and this may account for our accurate results.

We take a closer look at the natural orbitals in Figure 8. The impurity in this case is the right dimer. One may expect the first and second excitation to be the $\sigma^* \leftarrow \sigma$ transition in the H_2 dimer on the right dimer. A closer inspection of the natural orbitals shows that this is the case for the first excitation, but the second excitation is actually the $\sigma^* \leftarrow \sigma$ transition on the middle dimer. Hence, if we wanted to calculate an isolated, two electron excitation on the right dimer, it is not as easy as selecting the second excitation since the excitation leaks into the bath.

H #	FCI	SCF Soln 0	SCF Soln 1	SCF Soln 2	SCF Soln 3	SCF Soln 4
1	0.973547	0.995075	0.975885	0.823750	1.178580	0.992433
2	0.974468	1.004950	0.970767	0.829104	1.153560	0.981764
3	0.989980	0.998195	0.999586	1.239050	0.738844	1.115720
4	0.989050	1.001580	0.971201	1.236410	0.750481	1.137250
5	1.040294	1.010180	1.021720	0.941864	1.080620	0.895229
6	1.032661	0.990017	1.060850	0.929825	1.097910	0.877601
d	0	3.50351	3.50804	4.00347	4.00659	4.48754

TABLE I. Populations on each hydrogen atom as numbered in Figure 1 at $r = 1.00$ Å. d is the distance metric between each solution 1-RDM with the FCI 1-RDM as defined in Equation (35). SCF Soln denotes the result from the SCF solutions, starting from the lowest and moving to the fifth lowest SCF solution. We note that the populations obtained from the second lowest SCF solution is the best match to the FCI populations.

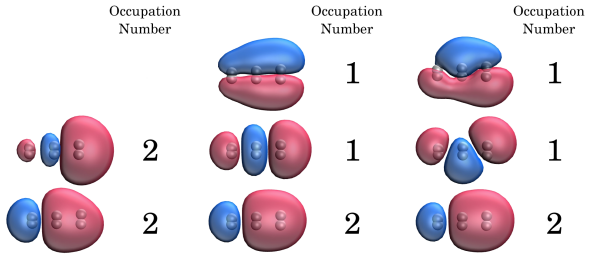

FIG. 7. The natural orbitals of the impurity calculation and their corresponding occupation numbers for the lowest (left), second lowest (middle), and third lowest (right) impurity CI solution at $r = 1.25$ Å.

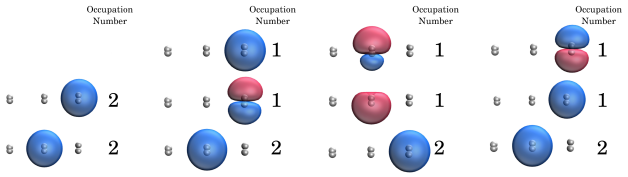

FIG. 8. The natural orbitals of the impurity calculation and their corresponding occupation numbers for the lowest (left), second lowest (middle left), third (middle right), and fourth (right) lowest impurity CI solution at $r = 3.00$ Å.

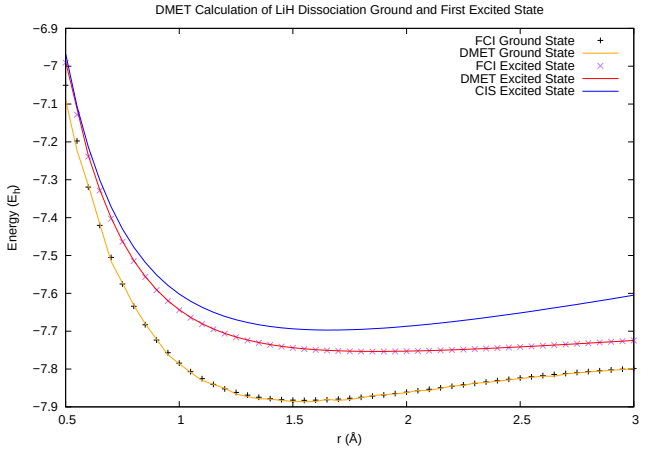

FIG. 9. The FCI ground state energy (black), FCI first singlet excited state energy (purple), DMET ground state energy (orange), and DMET first excited state energy (red) of LiH dissociation. Singlet excited state energies using CIS (blue) is also plotted for comparison.

C. Lithium Hydride Results

The second system in this study is the lithium hydride dimer. We calculate the ground and first singlet excited state along the dissociation coordinate, labeled r. Note that the dissociation coordinate is aligned along the z axis. The bond length is varied from 0.50 Å to 3.00 Å in steps of 0.05 Å. The basis set used is the Löwdin symmetrically orthogonalized STO-3G basis, the same as described in Section IV A. The system is tiled into four impurities. Impurity 1 contains the localized 1s and 2s orbitals on lithium. Impurity 2 contains the localized $2p_x$ orbital on lithium. Impurity 3 contains the localized $2p_y$ orbital on lithium. Impurity 4 contains the localized $2p_z$ orbital on lithium and the localized 1s orbital on the hydrogen. In this case, we optimize the correlation potential, $\hat{u}$.

For the first excited state, the ground SCF solution is used as the bath state, rather than the first excited SCF solution because the first excited SCF solution obtained from SCF metadynamics appears to be a charge transfer from hydrogen to lithium, which goes against our intuition for the nature of the excitation. The reference 1-RDM in Equation (33) is the first excited Δ-SCF UHF solution when the Li $2p_x$ and $2p_y$ orbitals are forced to be unoccupied. The energy was calculated at a reference geometry with this choice of bath state and reference 1-RDM. This solution was followed along the energy curve.

The results of the ground state and first singlet excited state calculations using DMET are plotted in Figure 9. The FCI energies for these states are also plotted for reference. The CIS singlet excited state is plotted for comparison. We find that both the ground and excited state DMET calculations agree exceptionally well with the FCI calculation. In particular, excited state DMET does much better qualitatively and quantitatively than the CIS calculation. This indicates that excited state DMET again recovers a significant amount of correlation in this system.

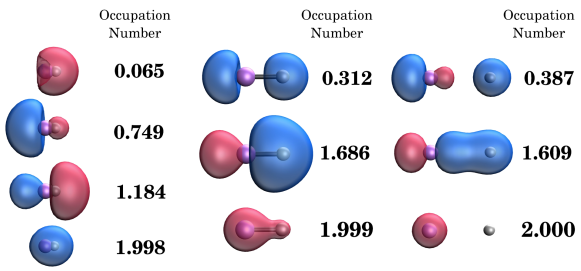

FIG. 10. The occupied natural orbitals and their occupation numbers of the first singlet excited state of LiH at $r = 0.50$ Å (left), $r = 1.50$ Å (middle), and $r = 3.00$ Å (right). These orbitals are obtained from the FCI solution for the first singlet excited state at each of these geometries.

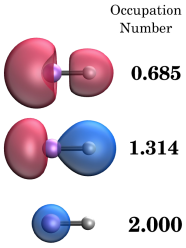

FIG. 11. The natural orbitals of the impurity calculation and their corresponding occupation numbers for the impurity CI solution used in the calculation at $r = 1.50$ Å. The impurity orbitals are the localized Li $2p_z$ and H 1s orbitals.

D. Lithium Hydride Discussion

1. *Nature of Excitation*

We examine the occupied natural orbitals (occupation number greater than 10^{-2}) and their occupation numbers at $r = 0.50$ Å, $r = 1.50$ Å, and $r = 3.00$ Å for the first singlet excited state. These are pictured in Figure 10. From this figure, we find that along all geometries, the excitation is mostly a $\sigma^* \leftarrow \sigma$ transition involving the Li $2p_z$ and H 1s orbitals.

This character should be seen in Impurity 4. The natural orbitals and their occupations of the impurity calculation for Impurity 4, for the impurity excitation used in the calculation, is plotted in Figure 11. We see the same $\sigma^* \leftarrow \sigma$ transition as we saw in the full system FCI excitation in Figure 10. One point to note is that the occupations of these natural orbitals differ from the occupations predicted in the FCI calculation. However, even with this discrepancy, we find that the excited state DMET calculation does a good job predicting the excited state energy.

We also emphasize that the partial occupation character of the excited state is recovered by impurity calculation, similar to what was discussed in Section IV B 3. This allows us to predict a complicated excited state starting from a closed shell RHF state.

	FCI	SCF Soln 0	SCF Soln 1	SCF Soln 2
Li 1s	1.999197	1.999420	1.998840	1.998110
Li 2s	0.572317	0.492116	1.807780	0.001328
Li $2p_x$	0.000933	0.000000	0.000000	1.753360
Li $2p_y$	0.000933	0.000000	0.000000	0.246643
Li $2p_z$	0.353861	0.160965	0.021956	0.000141
H 1s	1.072759	1.347500	0.171427	0.000421
d	0	2.54190	2.62615	2.99964

TABLE II. Populations on each localized atomic orbital of LiH at $r = 1.50$ Å. The FCI result is for the first singlet excited state. d is the distance metric between each solution 1-RDM with the FCI 1-RDM as defined in Equation (35). SCF Soln denotes the result from the SCF solutions, starting from the lowest and moving to the third lowest SCF solution. We note that the populations obtained from the lowest SCF solution is the best match to the FCI populations.

2. *Assessing State Selection*

For LiH, we found the ground SCF solution to be the preferred starting point over higher lying SCF solutions. As was discussed in Section IV B 2, it seems the population on each orbital is a good indicator of the quality of an SCF solution. Table II shows that the ground SCF solution indeed best represents the FCI populations.

It raises a concern that a different choice of SCF state was used to target the same type of excited state in two different systems. Such an ambiguity is expected with SCF metadynamics, which exhaustively obtains all SCF solutions. We emphasize the same points in Section IV B 2 that the choice of bath state will likely be easier if a more flexible theory (UHF or ROHF) is applied, rather than closed shell RHF, and a state targeting mean-field method is used, rather than SCF metadynamics.

For this system, we find that higher lying UHF solutions are once again adequate for providing the reference 1-RDM. Moving forward, UHF solutions may no longer be adequate for more complicated systems. Even in this system, the UHF solution had to be modified to restrict occupation into the Li $2p_x$ and $2p_y$ orbitals. Future work may explore more accurate, but still low scaling, methods to produce the reference 1-RDM.

Again, we reiterate the point in Section IV B 2 that our comparison to a reference 1-RDM is a trivial choice of metric. A better metric that is not as closely tied with improving the full system calculation would be a great advancement for excited state embedding. We hope that the initial success in these systems encourages work towards this endeavor.

V. CONCLUSION

In this work, we present a framework towards calculating the excited states of molecular systems with the computational efficiency of quantum embedding methods. We apply the DMET[18,19,21] prescription for quantum embedding and take advantage of higher lying SCF solutions, found using a method inspired by metadynamics,[17] to directly calculate ex-

cited state energies. In contrast to other works on calculating excited state properties using DMET,[26,36] our formulation specifically obtains the excited state energies. Initial results were obtained for a model system of hydrogen dimers and the lithium hydride dissociation. The excited states were accurately predicted for these small systems using our methodology. We acknowledge the difficulties in choosing the bath state for the embedding and the reference 1-RDM to distinguish between the impurity states. We offer suggestions moving forward, but our work has demonstrated that excited state DMET is at least possible.

We find success in a system of three H_2 dimers, in the limit of weak and strong coupling. We are able to reproduce the first singlet excited state energy with good accuracy in both these limits. The excitation in this system is found to be delocalized outside of the boundary of the impurity, where an embedding method would be expected to fail. The dissociation curve of LiH was also studied and the two lowest lying singlet electronic states were accurately reproduced. By comparing with CIS, we see that DMET recovers significant correlation in the excited states. However, we acknowledge that when moving beyond these small systems, the excited state DMET procedure will likely require substantial improvements to achieve the same quality of results.

The first pitfall is the ambiguity in which SCF state should be used to represent the excited state of interest and be the target of the Schmidt decomposition. Higher lying SCF solutions obtained from SCF metadynamics was used in this work with success. However, even in the two small systems we studied, there was still a discrepancy on which SCF state should be chosen to target the first excited state (first excited SCF state for the H_2 dimers and ground SCF state for LiH). This problem will only get worse for larger systems. A lot of this ambiguity comes from the fact that SCF metadynamics is stochastic with the intention of exhaustively searching the solution space. An SCF metadynamics calculations returns, in principle, all SCF solutions so choosing between them is very difficult. More befitting of our formulation of excited state DMET are targeted mean-field methods with the goal of obtaining one specific solution. This will greatly reduce the ambiguity between bath states. These methods include Δ-SCF,[14] σ-SCF,[15] and half-projected σ-SCF.[16] These methods should be explored as alternatives for more complicated systems.

Moreover, improving the DMET calculation relies on improving the initial mean-field calculation on the full system. A more flexible theory such as UHF or ROHF as the starting point for the Schmidt decomposition should allow DMET to be applied to larger molecules and target more complicated electronic states.

The second pitfall is the ambiguity in which impurity state should be chosen to target the intended excited state. This is avoided in ground state DMET as it should always be the ground impurity state. To conquer this issue, we must have a metric that distinguishes between impurity states and singles out the best state. We introduce a "trivial" metric of matching 1-RDMs to some reference 1-RDM as described in Equation (33). This was successful for our small systems when higher lying UHF solutions were used to produce the reference 1-RDM. This is unlikely to be as successful for larger systems where UHF is no longer qualitatively accurate. The clearest path to improvement is improving the reference, but that requires a more accurate calculation on the full system. There is still room for improvement as UHF was used for this work, which is one of the cheapest methods available, but this is not the ideal way forward. The purpose of our results is to demonstrate that impurity states can be chosen to predict excite state energies and the trivial metric served this purpose. Further work in developing a better scaling metric could find good use in excited state DMET, as shown by our initial results.

This framework offers a potential direction to improve DMET in general. In this work, an SCF solution is chosen and a Schmidt decomposition is performed to obtain the entangled bath states for each impurity. Then the impurity calculation is performed in the space of fragment and entangled bath orbitals. The set of entangled bath orbitals changes with the choice of SCF solution and one way to improve the impurity calculation is to augment the active space with entangled bath orbitals from all SCF solutions, instead of just using bath orbitals from one SCF solution. This will allow us to expand the impurity space and perhaps allow DMET to capture dynamic correlation.[29] This is an interesting direction that builds off of the framework presented in this work, but it is not directly related to excited state calculations and will be left as future work.

The work in this paper marks the first extension of DMET to directly embed excited states. Although one may expect this to be straightforward, our work points out key features of such an embedding method including important pitfalls that one must be wary of in attempting such an embedding theory. This discussion has shown that the method of excited state DMET has many more degrees of freedom than one may initially imagine, and its application is certainly not trivial. The biggest difficulty is how one determines the best bath and impurity solution to use in the DMET prescription. However, our results show that excited state DMET is possible. Future work in this direction should tackle the problems that arose in this study and we have suggested improvements in the method that will help reduce the ambiguity in state selection.

VI. ACKNOWLEDGEMENTS

HKT acknowledges support from the Winston Churchill Foundation of the United States and the NSF GRFP. TV contributed to the state selection procedure. His work was supported by a grant from the NSF (CHE-1464804). AJWT thanks the Royal Society for a University Research Fellowship (Grants UF110161 and UF160398).

[1] P. Hohenberg and W. Kohn, "Inhomogeneous Electron Gas," Phys. Rev. **136**, B864 (1964).
[2] W. Kohn and L. Sham, "Self-Consistent Equations Including Exchange and Correlation Effects," Phys. Rev. **140**, A1133 (1965).
[3] E. Runge and E. K. U. Gross, "Density-Functional Theory for Time-Dependent Systems," Phys. Rev. Lett. **52**, 997–1000 (1984).
[4] M. A. L. Marques and E. K. U. Gross, "Time-Dependent Density-Functional Theory," Annu. Rev. Phys. Chem. **55**, 427 (2004).

[5] F. Furche and K. Burke, "Time-dependent density functional theory in quantum chemistry," Annu. Rep. Comp. Chem. **1**, 19–30 (2005).

[6] N. T. Maitra, K. Burke, H. Appel, and E. K. U. Gross, "Ten topical questions in time-dependent density functional theory," Rev. Mod. Q. Chem. (2001).

[7] A. J. Cohen, P. Mori-Sanchez, and W. Yang, "Insights into Current Limitations of Density Functional Theory," Science **321**, 792–794 (2008).

[8] C. Adamo and D. Jacquemin, "The calculations of excited-state properties with Time-Dependent Density Functional Theory," Chem. Soc. Rev. **42**, 845–856 (2013).

[9] I. Shavitt, "The history and evoluton of configuration interaction," Mol. Phys. **94**, 3–17 (1998).

[10] J. F. Stanton and R. J. Bartlett, "The equation of motion coupled-cluster method. a systematic biorthogonal approach to molecular excitation energies, transition probabilities and excited state properties," J. Chem. Phys. **98**, 7029 (1993).

[11] A. Szabo and N. S. Ostlund, *Modern Quantum Chemistry: Introduction to Advanced Electronic Structure Theory* (Dover Books, 1989).

[12] C. C. J. Roothaan, "New Developments in Molecular Orbital Theory," Rev. Mod. Phys. **23**, 69–89 (1951).

[13] O. Gunnarsson and B. I. Lundqvist, "Exchange and correlation in atoms, molecules, and solids by the spin-density-functional formalism," Phys. Rev. B. **13**, 4274 (1977).

[14] J. Gavnholt, T. Olsen, M. Engelund, and J. Schiotz, "Delta Self-Consistent Field as a method to obtain potential energy surfaces of excited molecules on surfaces," Phys. Rev. B **78**, 075441 (2008).

[15] H.-Z. Ye, M. Welborn, N. D. Ricke, and T. Van Voorhis, "σ-scf: A direct energy-targeting method to mean-field excited states," The Journal of Chemical Physics **147**, 214104 (2017), https://doi.org/10.1063/1.5001262.

[16] H.-Z. Ye and T. Van Voorhis, "Half-projected σ-self-consistent field for electronic excited states," Journal of Chemical Theory and Computation **15**, 2954–2965 (2019), pMID: 30995060, https://doi.org/10.1021/acs.jctc.8b01224.

[17] A. J. W. Thom and M. Head-Gordon, "Locating Multiple Self-Consistent Field Solutions: An Approach Inspired by Metadynamics," Phys. Rev. Lett. **101**, 193001 (2008).

[18] G. Knizia and G. K.-L. Chan, "Density Matrix Embedding: A Simple Alternative to Dynamical Mean-Field Theory," Phys. Rev. Lett. **109**, 186404 (2012).

[19] G. Knizia and G. K.-L. Chan, "Density Matrix Embedding: A Strong-Coupling Quantum Embedding Theory," J. Chem. Theory Comput. **9**, 1428–1432 (2013).

[20] I. Peschel and V. Eisler, "Reduced density matrices and entanglement entropy in free lattice models," J. Phys. A: Math. Theor. **42**, 504003 (2009).

[21] B.-X. Zheng and G. K.-L. Chan, "Ground-state phase diagram of the square lattice Hubbard model from density matrix embedding theory," Phys. Rev. B: Condens. Matter Mater. Phys. **93**, 035126 (2016).

[22] T. Tsuchimochi, M. Welborn, and T. Van Voorhis, "Density matrix embedding in an antisymmetrized genimal power bath," J. Chem. Phys. **143**, 024107 (2015).

[23] Z. Fan and Q. lin Jie, "Cluster density matrix embedding theory for quantum spin systems," Phys. Rev. B: Condens. Matter Mater. Phys. **91**, 195118 (2015).

[24] K. Gunst, S. Wouters, S. D. Baerdemarcker, and D. Van Neck, "Block product density matrix embedding theory for strongly correlated spin systems," Phys. Rev. B **95**, 195127 (2017).

[25] I. W. Bulik, W. Chen, and G. E. Scuseria, "Intermediate and spin-liquid phase of the half-filled honeycomb Hubbard model," J. Chem. Phys. **141**, 054113 (2014).

[26] Q. Chen, G. H. Booth, S. Sharma, G. Knizia, and G. K.-L. Chan, "Intermediate and spin-liquid phase of the half-filled honeycomb Hubbard model," Phys. Rev. B: Condens. Matter Mater. Phys. **89**, 165134 (2014).

[27] M. Welborn, T. Tsuchimochi, and T. Van Voorhis, "Bootstrap embedding: An internally consistent fragment-based method," J. Chem. Phys. **145**, 074102 (2016).

[28] N. Ricke, M. Welborn, H.-Z. Ye, and T. Van Voorhis, "Performance of Bootstrap Embedding for long-range iinteraction and 2D systems," Mol. Phys. , 1–12 (2017).

[29] H.-Z. Ye, M. Welborn, N. D. Ricke, and T. Van Voorhis, "Incremental embedding: A density matrix embedding scheme for molecules," preprint (2018), https://arxiv.org/abs/1807.08863, arXiv:1807.08863.

[30] I. W. Bulik, G. E. Scuseria, and J. Dukelsky, "Density matrix embedding from broken symmetry lattice mean fields," Phys. Rev. B **89**, 035140 (2014).

[31] B. Sandhoefer and G. K.-L. Chan, "Density matrix embedding theory for interacting electron-phonon systems," arXiv:1602.04195 (2016).

[32] J. LeBlanc, A. Antipov, F. Becca, I. Bulik, G. Chan, C.-M. Chung, Y. Deng, M. Ferrero, T. Henderson, C. Jiménez-Hoyos, E. Kozik, X.-W. Liu, A. Millis, N. Prokofiev, M. Qin, G. Scuseria, H. Shi, B. Svistunov, L. Tocchio, I. Tupitsyn, S. R. White, S. Zhang, B.-X. Zheng, Z. Zhu, and E. Gull, "Solutions of the Two-Dimensional Hubbard Model: Benchmarks and Results from a Wide Range of Numerical Algorithms," Phys. Rev. X **5**, 041041 (2015).

[33] S. Wouters, C. A. Jimenez-Hoyos, Q. Sun, and G. K.-L. Chan, "A Practical Guide to Density Matrix Embedding Theory in Quantum Chemistry," J. Chem. Theory Comput. **12**, 2706–2719 (2016).

[34] Q. Sun and G. K.-L. Chan, "Exact and Optimal Quantum Mechanics/Molecular Mechanics Boundaries," J. Chem. Theory Comput. **10**, 3784–3790 (2014).

[35] S. Sorella, N. Devaus, M. Degrada, G. Mazzola, and M. Casula, "Geminal embedding scheme for optimal atomic basis set construction in correlated calculations," J. Chem. Phys. **143**, 244112 (2015).

[36] G. H. Booth and G. K.-L. Chan, "Spectra functions of strongly correlated extended systems via an exact quantum embedding," Phys. Rev. B **91**, 155107 (2015).

[37] A. T. B. Gilbert, N. A. Besley, and P. M. W. Gill, "Self-Consistent Field Calculations of Excited States Using the Maximum Overlap Method (MOM)," J. Phys. Chem. **112**, 13164–13171 (2008).

[38] A. J. W. Thom and M. Head-Gordon, "Hartree-Fock solutions as a quasidiabatic basis for nonorthogonal configuration interaction," J. Chem. Phys. **131**, 124113 (2009).

[39] A. Pathak, *Elements of Quantum Computatoin and Quantum Communication* (Taylor and Francis, 2003).

[40] D. Janzing, *Compendium of Quantum Physics* (Springer Berline Heidelberg, 2009).

[41] J. C. Slater, "The Theory of Complex Spectra," Phys. Rev. **34**, 1293 (1929).

[42] C. C. J. Roothaan, "Self-consistent field theory for open shells of electronic systems," Rev. Mod. Phys. **32**, 179–185 (1960).

[43] H. Fukutome, "Unrestricted hartree–fock theory and its applications to molecules and chemical reactions," Int. J. Quantum Chem. **20**, 955–1065 (1981), https://onlinelibrary.wiley.com/doi/pdf/10.1002/qua.560200502.

[44] A. Laio and M. Parrinello, "Escaping free-energy minima," Proc. Natl. Acad. Sci. **99**, 12562 (2002).

[45] W. J. Hehre, R. F. Stewart, and J. A. Pople, "Self-Consistent Molecular-Orbital Methods. I. Use of Gaussian Expansions of Slater-Type Atomic Orbitals," J. Chem. Phys. **51**, 2657 (1969).

[46] P. O. Lowdin, "Quantum Theory of Many-Particle Systems. I. Physical Interpretations," Phys. Rev. **97**, 1474 (1955).

[47] Q. Sun, T. C. Berkelbach, N. S. Blunt, G. H. Booth, S. Guo, Z. Li, J. Liu, J. D. McClain, E. R. Sayfutyarova, S. Sharma, S. Wouters, and G. K.-L. Chan, "Pyscf: the python-based simulations of chemistry framework," WIREs Comput Mol Sci **8**, e1340 (2017), https://onlinelibrary.wiley.com/doi/pdf/10.1002/wcms.1340.

[48] G. Guennebaud, B. Jacob, *et al.*, "Eigen v3," http://eigen.tuxfamily.org (2010).